Applied Catalysis A, General 591 (2020) 117385

Contents lists available at ScienceDirect

Applied Catalysis A, General

journal homepage: www.elsevier.com/locate/apcata

An unconventional DCOx favored Co/N-C catalyst for efficient conversion of fatty acids and esters to liquid alkanes

Jiang Li[a,*], Jiaxing Liu[a], Junjie Zhang[a], Tong Wan[a], Lei Huang[a], Xintian Wang[a], Runze Pan[a], Zhidong An[a], Dionisios G. Vlachos[b,*]

[a] State Key Laboratory of Heavy Oil Processing, China University of Petroleum (Beijing), Beijing 102249, China
[b] Department of Chemical and Biomolecular Engineering and Catalysis Center for Energy Innovation, University of Delaware, 221 Academy St., Newark, DE 19716, United States

ARTICLE INFO

Keywords:
Biomass conversion
Fatty acid and ester
Cobalt
Heterogeneous catalysis
Selectivity regulation

ABSTRACT

Cobalt (Co) catalysis has recently attracted significant attention in the field of biomass conversion. However, the fabrication of highly dispersive Co nanoparticles at high metal loading with selective facet exposure to achieve specific selectivity is still questionable. In this work, a nitrogen-doped carbon-supported Co catalyst is fabricated for efficient conversion of fatty acids and esters to liquid alkanes. Nitrogen-doping facilitates a highly uniform dispersion of Co nanoparticles even at a high Co loading of 10 wt% and after recycling for 5 runs. The Co/N-C catalyst affords an unconventional decarbonylation/decarboxylation (DCOx) dominant selectivity probably due to partial reduction of cobalt oxides to α-Co^0 with only exposure of the (111) facet. Co-existence of Co and N-C leads to strong Lewis acidity and basicity, facilitating the interaction between catalyst and –COOH group, and some important acid-catalyzed step-reactions. The versatility of the Co/N-C catalyst is demonstrated through conversion of various fatty acids and esters.

1. Introduction

Triglycerides, which are esters of glycerol with three long-chain fatty acids, are an important biomass-derived sustainable feedstock for biofuel production [1]. The transesterification of triglycerides with methanol produces fatty acid methyl esters (FAME), which is well known as first generation biodiesel, with an annual manufacture throughput of more than 20 million tons [2]. However, the relatively high oxygen content, poor low-temperature flow properties, and unsatisfactory thermal and oxidation stability prevent it from being a high-grade fuel in current engines [3]. Hence, direct conversion of triglycerides into diesel-range alkanes (C15-C18) has recently attracted significant attention.

Alkanes are generally produced from triglycerides using two types of catalysts. Conventional hydrotreating, refinery catalysts, such as sulfide CoMo and NiMo catalysts, have been proposed as highly active catalysts for this reaction [4–6]. However, the sulfur contamination of alkane products by unavoidable catalyst leaching, the addition of sulfiding agents to the liquid feed to avoid catalyst deactivation, and the enhanced sulfur leaching by trace amount of water produced in the reactions remain key challenges. As a result, sulfur-free supported metal catalysts for triglyceride conversion has recently attracted significant attention. Two impressive studies reported by Lercher and coworkers successfully tuned the product distribution using HBeta and ZrO_2-supported Ni catalysts [7,8]. Inspiring by their findings, various catalysts have been reported. Compared to noble metals, such as Pd [9], Pt [10], Ru [11–13], and Ir-ReOx [14], non-noble metals such as Ni [15–19], Co [20–24], W [25], Mo [26,27], and Fe [28,29] are more attractive in terms of economics and abundance.

Cobalt (Co) has recently emerged as an attractive metal center for biomass conversion. Various reactions, such as 5-hydroxymethylfurfural (HMF) oxidation [30] or reductive etherification [31], hydrogenation of levulinic acid to gamma-valerolactone or valeric biofuel [32,33], bio-oil-derived molecule upgrade [34,35], furfural hydrogenation [36], and oxidative cleavage of lignin β-O-4 model compounds [37] have been realized over Co catalysts. However, the fabrication of highly dispersive Co nanoparticles at high loading with selective facet exposing is still questionable, which is important to achieve enhanced activity and specific selectivity. For triglycerides conversion, Co is usually combined with Ni for tailoring product distribution [20–22]. As shown in Scheme 1, the conversion of triglycerides-based fatty acids usually involves two types of reactions: decarbonylation/decarboxylation (DCOx) and hydrodeoxygenation (HDO). DCOx produces alkanes with one less carbon atom, whereas HDO

* Corresponding authors.
E-mail address: lijiang@cup.edu.cn (J. Li).

https://doi.org/10.1016/j.apcata.2019.117385
Received 14 August 2019; Received in revised form 20 December 2019; Accepted 23 December 2019
Available online 23 December 2019
0926-860X/

DCOx:

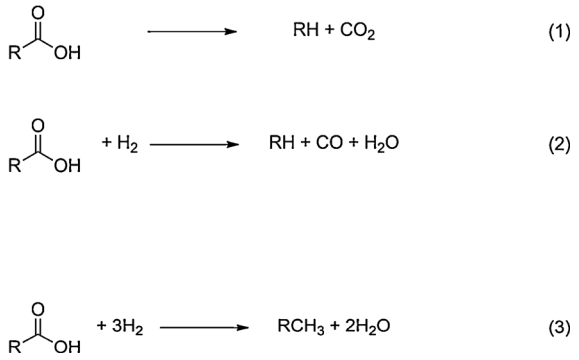

HDO:

Scheme 1. Conversion of fatty acids to alkanes via decarboxylation (Path 1) or decarbonylation (Path 2), abbreviated collectively as DCOx, or hydrodeoxygenation (HDO) (Path 3).

preserves the number of carbon atoms. Although HDO affords better carbon atom economy and higher energy value of alkane products over DCOx, the consumption of H_2 in DCOx is relatively lower, making it less costly and more energy-efficient [8]. However, previous Co-based catalysts, e.g., Co/γ-Al_2O_3, Co/H-ZSM-5, and Co/clay, usually favor HDO over DCOx (Table S1) [20–23]. Despite Co/SiO_2 catalyst has represented a DCOx favored selectivity, the result is buried in many other HDO favored results over H-ZSM-22-supported Co catalysts, and the reason for such selectivity regulation is not even investigated [24]. Thus, it is still desirable to unravel the mechanism controlling selectivity to rationally develop DCOx favored Co catalysts.

Nitrogen-doping has recently been recommended as an effective way to improve the catalytic activity of cobalt catalyst. Beller and coworkers had reported pioneer work using Co/N-C catalysts towards organic synthesis, such as nitroarenes reduction, mild epoxidation of alkenes, selective oxidation of alcohol to esters, and hydrogenation of terminal and internal olefins [38–41]. This nitrogen-doping promotion effect has also been observed in some Co-catalyzed biomass conversions [30,34,35,37]. The nitrogen dopant could introduce additional unpaired electrons to the conjugation of graphitic systems to facilitate electron transfer and substrate adsorption [42,43]. In this work, a nitrogen-doped carbon-supported Co catalyst with an average particle size of 7.0 nm is fabricated via simultaneous pyrolysis of cobalt(II) acetate and melamine onto activated carbon at 550 °C. Nitrogen-doping induces the formation of highly dispersed Co NPs even at a high Co loading of 10 wt% and after recycling tests. XRD showed that only the (111) facet of α-Co^0 is exposed at 550 °C, while additional (200) and/or (220) facets are exposed at higher pyrolysis temperatures. The selective exposure of the (111) facet of α-Co^0 renders a DCOx favored reaction route. The versatility of Co/N-C catalyst was successfully demonstrated by conversion of various fatty acids and esters, and plant oil.

2. Experimental section

2.1. List of chemicals

Metal oxide supports such as α-Al_2O_3 (99.9 %), TiO_2 (99 %), SiO_2 (99.9 %), and ZrO_2 (99 %), and solvents such as dodecane (98 %), and decane (98 %) were purchased from Aladdin Reagent Co. Ltd. Cobalt(II) acetate tetrahydrate (98.5 %) and ethanol (99.5 %) were purchased from Sinopharm Chemical Reagent Co. Ltd. Melamine (98 %), activated carbon (99 %), octadecane (98 %), 1-octadecene (90 %), octadecanol (98 %), and octadecanal (95 %) were purchased from TCI Development Co. Ltd.

2.2. Catalyst preparation

The Co/N-C catalysts were prepared by simultaneous pyrolysis of cobalt and nitrogen precursors onto various supports under Ar at 350 − 1100 °C. The cobalt loading is 10 wt% unless otherwise specified. Typical preparation is as follows: a certain amount of cobalt(II) acetate tetrahydrate was added into ethanol (100 mL) at room temperature. After a complete dissolution, melamine was added. Then activated carbon (1 g) was added, and the solution was stirred at 60 °C for 16 h followed by evaporation to remove the solvent. The solid was then dried at 60 °C overnight. The final precursor was grounded into fine powder, and then heated in a tubular furnace. An argon flow was used at a flow rate of 100 mL min^{-1}. The best Co/N-C catalyst is prepared according to following temperature program: 20 °C hold for 60 min, ramp 10 °C min^{-1} to 550 °C and then hold for 2 h. The catalysts are denoted as Co/(N)-S-T, where S represents the type of support, and T represents the pyrolysis temperature. The Co/N-C catalysts prepared from different batches exhibited the same catalytic performance, demonstrating that our preparation method is highly reproducible.

2.3. Catalyst characterization

The morphology was characterized by Hitachi SU8010 scanning electron microscopy (SEM, Japan) at 20 kV. (High-resolution) transmission electron microscopy (TEM or HRTEM) and high-angle annular dark field microscopy (HAADF-STEM) were performed on a JEOL JEM-2100 F high-resolution transmission electron microscope operated at 200 kV. N_2 adsorption measurements were performed on an ASAP2020 M adsorption analyzer. The surface areas of catalysts were calculated using the BET method in the range of relative pressures between 0.05-0.20. BJH method is used to calculate the pore size and distribution. XRD were operated on an X-ray diffractometer (TTR-III, Rigaku Corp., Japan) with Cu Kα radiation (λ = 1.54056 Å). XPS was performed on an X-ray photoelectron spectroscopy (ESCALAB 250Xi, Thermo-VG Scientific, USA) with monochromatized Al Kα radiation (1486.92 eV). The nitrogen content was detected by elemental analysis (Eurovector EA 3000). The cobalt content was detected by ICP-AES (Optima 7000DV, PerkinElmer Inc.). For NH_3- or CO_2-TPD tests, approximately 100 mg sample was loaded in a quartz reactor and then heated at 500 °C under argon flow for 2 h. The adsorption of NH_3 or CO_2 was done at 40 °C for 1 h, and then the catalysts were flushed with argon for 1 h. Subsequently, the sample was heated to 550 °C at a heating ramp rate of 10 °C min^{-1}. The desorbed NH_3 or CO_2 was measured by a gas chromatograph (GC) with a thermal conductivity detector (TCD). FTIR spectra were recorded on a Nicolet 8700 FTIR spectrometer in the wavenumber range from 400 to 4000 cm^{-1}. To explore the chemical adsorption of stearic acid on surface of Co/N-C-550 and Co/N-TiO_2-550 catalysts, the catalysts were treated as our previous studies. [13] 0.1 *g* catalyst was added into a 0.05 M stearic acid n-hexane solution (20 mL), and then the mixture was stirred at room temperature for 12 h. The solid was separated by centrifugation with 15 times washing of n-hexane. The final solid was dried at 80 °C overnight under N_2.

2.4. Experimental procedure

The conversion of fatty acids was operated in stainless reactors (50 mL) that purchased from Anhui Kemi Machinery Technology Co., Ltd. For a typical procedure, stearic acid (0.5 mmol), heterogeneous catalyst (100 mg), and alkane solvent (20 mL) were loaded into a quartz lining in the reactor. The reactor was then purged with hydrogen for three times, and then purged with 4 MPa H_2 at room temperature. The reaction was set at reaction temperature for 8 h with a stirring speed of 800 rpm. After reaction, the gaseous phase was analyzed by gas

chromatography (GC). A ShinCarbon ST 80/100 packed column (Restek) and a thermal conductivity detector (TCD) were used to determine the yields of H_2, CO, CO_2 and CH_4. A Plot Q column and a flame ionization detector (FID) were used to determine the yields of gaseous hydrocarbons such as CH_4, C_2H_6, and C_3H_8. The liquid products were collected, and eicosane (0.5 mmol) was added as internal standard. The products were analyzed using both gas chromatography (GC) and gas chromatography-mass spectrometry (GC–MS). GC–MS analysis was conducted by an Agilent 7890B Gas Chromatograph equipped with a HP-5MS 30 m × 0.25 mm × 0.25 μm capillary column (Agilent). The GC was directly interfaced to an Agilent 5977 mass selective detector (EI, 70 eV). A typical GC oven temperature program were listed as follows: 210 °C hold for 2 min, ramp 20 °C min^{-1} to 300 °C and hold for 2 min. Representative GC spectra are shown in supporting information (Figs. S1 and S2).

Some important experiments were operated at least twice to confirm reproducibility. The carbon loss can be attributed to the formation of undetected products in GC or cokes. For conversion of carboxylic acids, the conversion and yield were calculated by mol% as follows:

$$\text{Conversion} = \left(1 - \frac{\textit{molar amount of carboxylic acids after reaction}}{\textit{molar amount of carboxylic acids} \text{ before } \textit{reaction}}\right) \times 100\%$$

$$\text{Yield} = \frac{\text{molar amount of each product after reaction}}{\text{molar amount of carboxylic acids before reaction}} \times 100\%$$

The weight yield and total molar yields of liquid alkanes products for the conversion of plant oil were calculated as follows:

$$\text{Yield(wt\%)} = \frac{\textit{weight of each product after reaction}}{\textit{weight of cyperus esculentus oil} \text{ before } \textit{reaction}} \times 100\%$$

$$\text{Total yield(mol\%)} = \frac{\textit{total molar amounts of liquid alkanes after reaction}}{\textit{molar amounts of carboxylic acid groups} \text{ before } \textit{reaction}} \times 100\%$$

3. Results and discussion

3.1. Catalyst characterization

The Co catalysts were characterized using SEM, TEM, HRTEM, HAADF-STEM, and EDX elemental mapping. The SEM image of Co/N-C-550 catalyst shows irregular flakes (Fig. 1a) and carbon nanotubes with diameter of ca. 10 nm (Fig. 1b; see clearer TEM image in Fig. S3). The formation of carbon nanotubes is probably induced by the Co salt [44]. The TEM and HAADF images of Co/N-C-550 catalyst indicate highly dispersed Co NPs with an average particle size of 7.0 nm. In contrast, Co NPs in Co/C-550 catalyst are less uniform and larger in size (an average particle size is 24.7 nm, see Fig. S5). After five recycle runs, the Co NPs are still highly dispersed with average particle size of 16.2 nm (Fig. S6). The HRTEM image of Co/N-C-550 catalyst shows a lattice spacing of 2.06 Å corresponding to the (111) facet of α-Co^0, consistent with the XRD pattern (Fig. 2a). The particle size of Co NPs dramatically increases with increasing pyrolysis temperature (Figs. S8–S10). In contrast, no Co NPs form at 350 °C (Fig. S7). For Co catalysts prepared at 550 °C, increasing the Co loading to 30 wt% led to aggregation of Co NPs to particles of ca. 100 nm (Fig. S12), and the average particle size increased to 17.0 nm.

The XRD patterns of various catalysts are shown in Fig. 2. No characteristic peaks of Co species are observed for the Co/N-C-350 catalyst. The peak of the (111) facet of α-Co^0 at 44.2° (PDF#89-4307) is observed at a pyrolysis temperature of 550 °C. The (200) facet at 51.5° appears at 700 °C, and the additional (220) facet at 75.9° appears at pyrolysis temperature > 900 °C. In addition, the peak for graphitic carbon becomes sharper at pyrolysis temperature > 900 °C. For Co/N-C-550 catalysts, the increase in Co loading leads to an increase in the intensity of the peak of the (111) facet (Fig. 2b). The characteristic peak of Co species is not observed in the XRD patterns of metal oxide-supported Co catalysts except ZrO_2-supported catalyst (Fig. 2c). The characteristic peak of the (101) facet of β-Co (PDF#89-4308) at 47.4° is observed in the XRD pattern of the Co/C-550 catalyst.

The XPS spectra of Co/N-C catalysts prepared at different pyrolysis temperature are shown in Fig. 3. The N 1s spectra of N-C materials are usually fitted into four species: pyridinic N at 398.6 eV, pyrrolic N at 400.5 eV, graphitic N at 401.2 eV, and oxidized N at 402–405 eV [45,46]. In addition, a peak at 399.7 eV is observed in Co/N−C catalysts, which is assigned to bridge N in g-C_3N_4 (tertiary N bonded to carbon atoms in the form of N–$(C)_3$ or H–N–$(C)_2$) [47]. The N speciation is listed in Table S2. The total N content continuously decreases with increasing pyrolysis temperature, indicating the gradually reduced incorporation of nitrogen atoms in the catalyst during pyrolysis. The percentage content of bridge N also continuously decreases, showing that g-C_3N_4 forms at first [48] and gradually decomposes during pyrolysis, consistent with the C 1s XPS spectra (Fig. S13) and FTIR results (Fig. S14) [47]. The percent content of graphitic N continuously increases from 0 % to 82 % due to the Co-catalyzed graphitization of carbon.

The XPS spectra of Co 2p are shown in Fig. 3b. The two pair peaks at 779/793.6 and 781.6/796.8 eV correspond to Co^0/CoOx 2p 3/2 and 2p 1/2, respectively [49,50]. The peaks at 785.7 and 803.2 eV are satellite

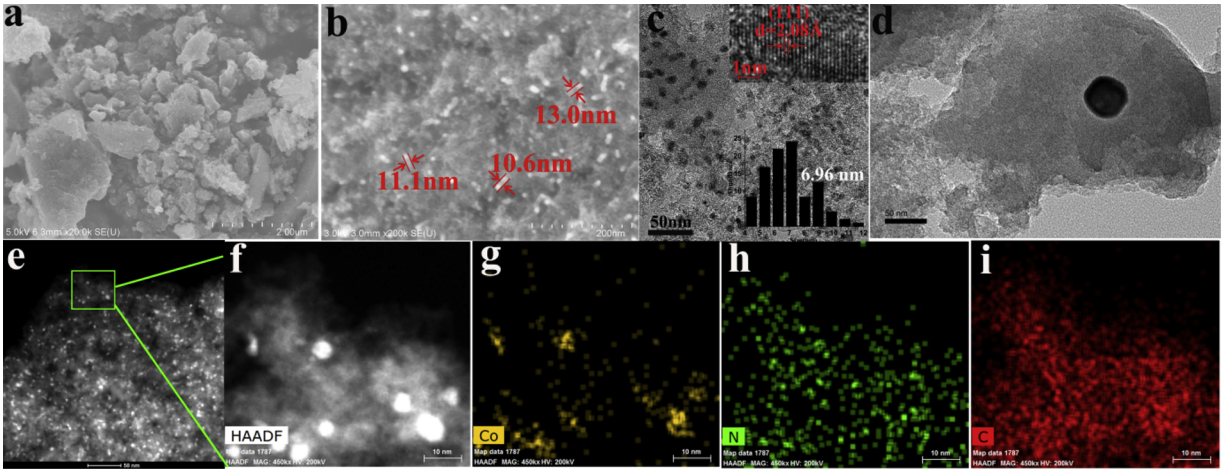

Fig. 1. SEM images (a, b), TEM image (c), HAADF-STEM (e, f), Co, N, and C elemental maps (g–i) of the Co/N-C-550 catalyst. (d) Typical TEM image of the Co/C-550 catalyst. The Co NPs size distribution and lattice distance (extracted from HRTEM image, see Fig. S3) are shown inside c.

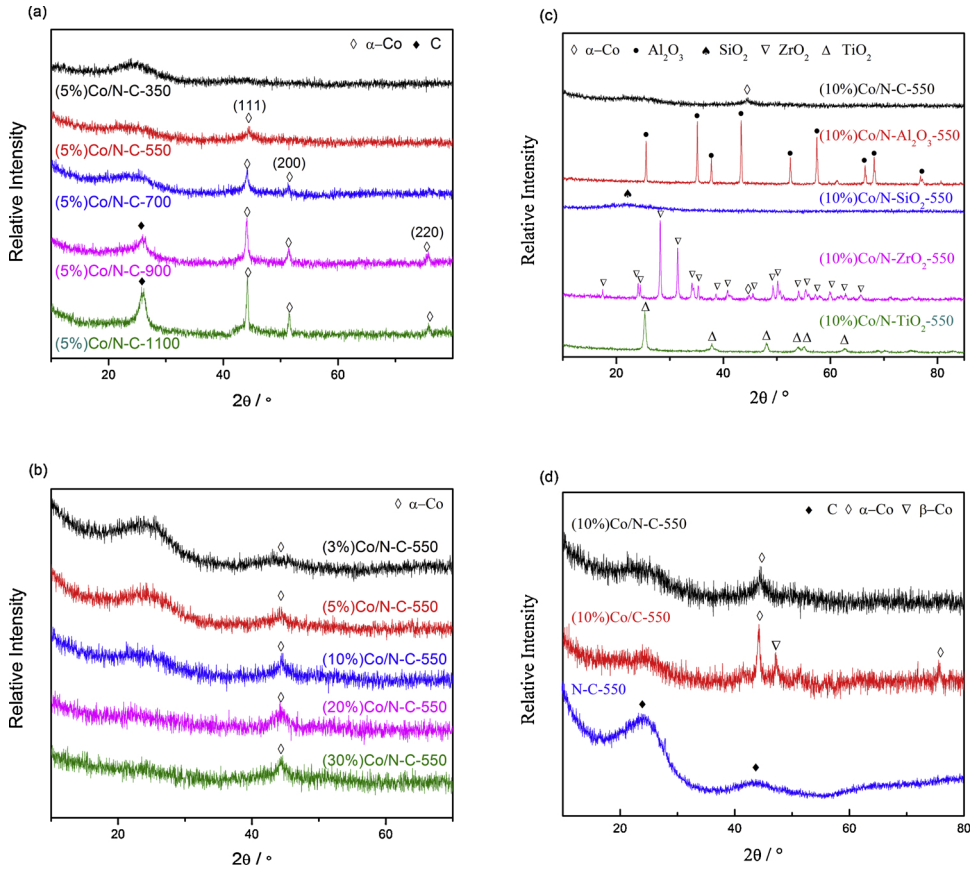

Fig. 2. XRD patterns of various catalysts. (a) Co/N-C catalysts prepared at different pyrolysis temperature. (b) Co/N-C catalysts with different Co loadings. (c) Co catalysts prepared on different supports. (d) Co/N-C, Co/C, and N-C catalysts.

peaks of Co 2p. It can be clearly seen that the Co^0 species appear at pyrolysis temperature > 550 °C, consistence with the XRD patterns. As metallic Co is easily oxidized in air, the N-doped carbon support retards the oxidization of Co^0 species and enhances its stability. The ratio of Co^0/CoOx species gradually increases with increasing pyrolysis temperature. Taken the characterization data together, the N-C support appears to stabilize smaller Co nanoparticles and prevent them from oxidation. These findings are consistent with recent density functional theory (DFT) calculations that indicate that N-C binds metal nanoparticles stronger and retards their agglomeration [51].

The N_2 sorption isotherms of various Co catalysts prepared at different pyrolysis temperature are shown in Fig. S15 and Table 1. The catalysts exhibit type IV isotherm at low relative pressures and an H4-type hysteresis loop around a relative pressure of 0.4–1.0 P/P_0, suggesting that they possess both micro- and meso-pores. The BET surface area and pore volume reach the highest value at 550 °C (Table 1). The BET surface area and pore volume of supported Co metal oxide catalysts are much lower whereas the average pore width is 2–4 times higher.

The Raman spectra clearly indicated the differences in the degree of graphitization in various carbon-based catalysts (Fig. 4, the ratios of D/G band are listed in Table S4). The Co/C-550 catalyst has a higher D/G band ratio than N-C-550 catalyst (1.26 vs 0.83), demonstrating that the loading of Co NPs generates more defects in carbon materials. By comparison, the co-loading of Co and N at 550 °C affords D/G band ratio of 1.15, illustrating that additional nitrogen-doping leads to less defects. The intensity ratio of D/G band decreased to 0.98 at 700 °C, and then inceased to 1.27 at temperature above 900 °C.

In summary, the characterization clearly shows that carbon-supported highly dispersed, partially reduced α-Co^0 NPs with only exposure of (111) facet are fabricated through simultaneous pyrolysis of Co salts and melamine onto activated carbon at 550 °C. The effect of synthesis conditions such as pyrolysis temperature, Co loading, and support on reactivity is examined below, and is correlated to their Lewis acidity and basicity.

3.2. Catalyst screening

Stearic acid is commonly used as a model compound to examine the activities of catalysts towards fatty acids conversion. Thus, the conversion of stearic acid is selected as a model reaction to assess the performance of various Co catalysts. All the reactions are performed in a glass vial to exclude the influence of the metallic reactor body. The results are summarized in Table 2. Here n-C18 refers to the alkane formed by HDO of stearic acid (Path 3 in Scheme 1), n-C17 to the one formed by DCOx (Paths 1 or 2 in Scheme 1), and C18−OH and C17−CHO to the corresponding alcohol and aldehyde formed by reduction of the acid. It should be noted that unsatisfactory carbon balance was observed in some experiments, which is probably due to the formation of GC undetected products such as cokes. A blank test indicates no reaction without a catalyst (Table 2, entry 1). Co catalysts can give significantly high yield to alkanes. No alcohol by-products are detected at 550 °C, and the yield to all alkanes reaches ~85 % with a highest C17/C18 ratio of 1.4 for the (5 %)Co/N-C-550 catalyst (entry 3). As stated before, only the (111) facet of α-Co^0 is exposed at 550 °C. The (200) and (220) facets are also co-exposed with the (111) facet at pyrolysis temperatures above 700 and 900 °C, respectively. The exposure of these facets leads to a decrease in the C17/C18 ratio. Previous literature on Co-catalyzed fatty acid conversion is consistent with our findings. Specifically, a Co/SiO_2 catalyst, which exposes only the (111) facet of α-Co^0, leads predominant to DCOx of the palmitic acid [24]. A $Co\text{-}Al_2O_3$ catalyst, which exposes the (200) facet after pre-reduction, leads to comparable DCOx and HDO selectivity [20]. Thus, our results

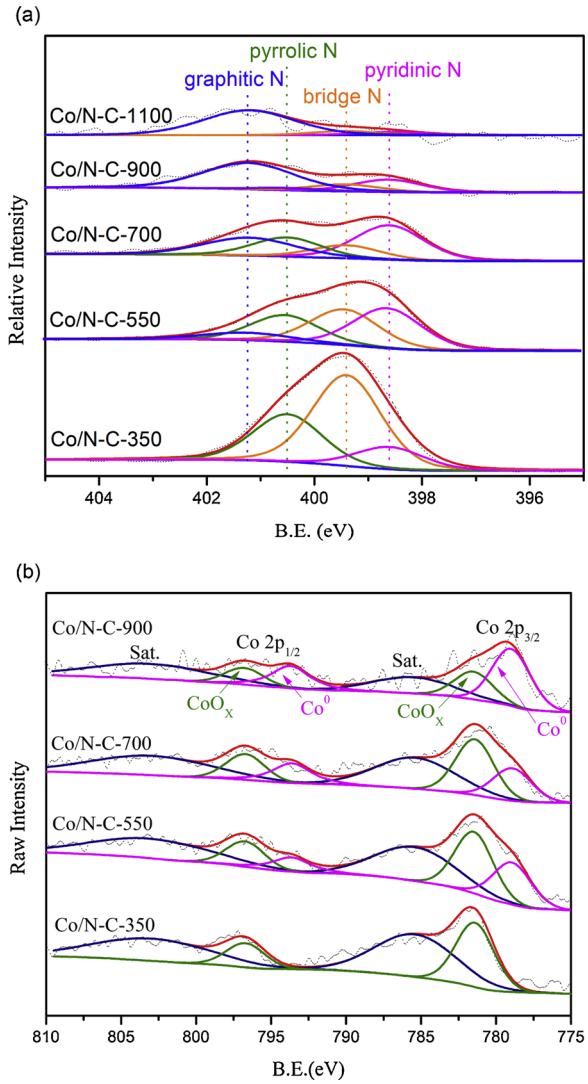

Fig. 3. N 1s (a) and Co 2p (b) XPS spectra of Co/N-C catalysts prepared at different pyrolysis temperatures.

Table 1
Textural properties of various cobalt catalysts.

Entry	Catalyst	BET Surface Area (m^2/g)	Pore Volume (cm^3/g)	Average Pore Width (nm)
1	Co/N-C-350	762	0.73	4.45
2	Co/N-C-550	1004	0.82	4.58
3	Co/N-C-700	1000	0.73	4.28
4	Co/N-C-900	856	0.73	4.61
5	Co/N-C-1100	659	0.68	5.01
6	Co/N-Al_2O_3	17	0.05	11.83
7	Co/N-SiO_2	156	0.77	21.45
8	Co/N-C-ZrO_2	9	0.04	13.28
9	Co/N-C-TiO_2	54	0.23	15.65

together with prior work suggest a strong correlation of the (111) facets of Co nanoparticles with DCOx selectivity. Such exposed plane-determined selectivity is also seen in reports by Wei et al., where the selectivity of the furfural hydrogenation is switched using Ni catalysts with different exposed planes [52]. However, probe molecule chemistry and extensive DFT calculations will be needed to better understand the relationship between exposed facet and selectivity as part of future work. 1-octadecanol forms at yield > 26.5 % over Co/N-C catalysts prepared at pyrolysis temperature > 700 °C, indicating that these Co

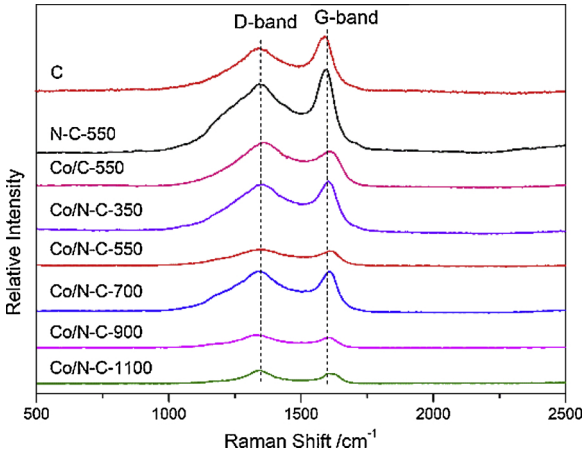

Fig. 4. Raman spectra of C, N-C-550, Co/C-550, and various Co/N-C catalysts.

catalysts are good hydrogenation catalysts but inferior for the conversion of 1-octadecanol to C18 or C17 alkanes.

The total yield to alkanes increases from 84.7 (entry 3) to 97.8 % (entry 8) when the Co loading increases from 5 to 10 wt%. Meanwhile, the C17/C18 ratio increases from 1.4 to 2.9. When the Co loading is raised to 30 wt%, the C17/C18 ratio reaches the highest value of 9.3 despite significant aggregation of Co NPs, suggesting that the particle size has no relationship with the C17/C18 ratio. Increase of the Co loading led to a gradual increase in the intensity of the peak for the (111) facet of α-Co^0, with no additional facets exposed, suggesting more DCOx products will be generated with more (111) facets. Meanwhile, slightly lower alkane yields are obtained with higher C17/C18 ratios. Due to the nearly quantitative yield achieved, a Co loading of 10 wt% is selected for subsequent experiments.

The replacement of alkane solvent with water leads to significantly lower conversion of stearic acid and yields of alkane products. When extracting alkane products from aqueous solution to determine their yields, the Co-N-C catalyst is found to be highly hydrophobic, dispersing better in alkane solvents. In addition, stearic acid is insoluble in water but soluble in hot alkanes. Hence, better contact of stearic acid with Co-*N*-C catalyst is achieved in alkane solvents than that in water during reaction, resulting in better catalytic performance of Co-*N*-C catalyst in alkane solvents.

Finally, the catalytic performance of (10 %)Co/C-550 and N-C-550 catalysts confirmed that both Co loading and nitrogen-doping are indispensable for the observed performance. The appearance of the (220) facet of α-Co^0 and the (111) facet of β-Co^0 in the XRD pattern of Co/C-550 catalyst, and the larger size and the lower size uniformity of Co NPs are responsible for low carbon balance and poor yields of alkanes. The absence of Co led to trace yields of product.

3.3. Effect of reaction temperature and H_2 pressure

The reaction temperature was varied in the range of 240 – 320 °C (Fig. 5a). From 320 to 280 °C, no alcohol by-products are detected and the carbon balance is excellent. A maximum C17/C18 ratio of 5.3 is achieved at 300 °C. At lower reaction temperatures, alcohol by-product forms and the carbon balance is lower. Consequently, a reaction temperature of 280 °C was used in subsequent experiments. In addition, the generation of alcohol at lower temperature also implicated that alcohol is probably the key intermediate during the conversion of stearic acid to alkanes.

The effect of H_2 pressure is summarized in Fig. 5b. No alcohol by-products are obtained even at H_2 pressure as low as 1 MPa. C17 is always produced as the major alkane product. As the H_2 pressure decreases from 4 MPa to 1 MPa, the C17/C18 ratio decreases from 3.5 to 1.6 and the conversion of stearic acid and carbon balance also slightly

Table 2
Catalyst screening for the conversion of stearic acid to alkanes.[a]

Entry	Catalysts	Conversion [%]	Yield[%]					C17/C18[b]	Carbon balance
			n-C17	n-C18	C18-OH	Cracking products	C17-CHO		
1	–	2.1	0.4	–	–	–	–	–	19.0
2	(5 %)Co/N-C-350	> 99.9	2.4	3.8	3.1	0.9	0	0.6(0.3)	10.2
3	(5 %)Co/N-C-550	> 99.9	48.7	34.7	0	1.3	0	1.4(1.4)	84.7
4	(5 %)Co/N-C-700	> 99.9	18.9	18.3	26.5	0.8	0	1.0(0.4)	64.5
5	(5 %)Co/N-C-900	> 99.9	14.4	24.8	35.7	0.9	0.1	0.6(0.2)	75.9
6	(5 %)Co/N-C-1100	> 99.9	14.9	17.1	36.9	0.9	0.7	0.9(0.3)	70.5
7	(3 %)Co/N-C-550	> 99.9	15.0	4.0	3.6	0.3	0	3.8(2.0)	22.9
8	(10 %)Co/N-C-550	> 99.9	70.2	24.4	0	3.2	0	2.9(2.9)	97.8
9	(20 %)Co/N-C-550	> 99.9	73.7	19.2	0	2.1	0	3.8(3.8)	95.0
10	(30 %)Co/N-C-550	> 99.9	81.5	8.8	0	3.7	0	9.3(9.3)	94.0
11[c]	(10 %)Co/N-C-550	18.6	0.2	0.06	4.2	0.17	0	3.3(0.05)	23.8
12	(10 %)Co/C-550	81.9	5.1	4.0	15.8	0.3	0	1.3(0.3)	30.8
13	N-C-550	22.4	0.8	0.2	0	0.3	0	4(4)	5.8

[a] Reaction conditions: 0.5 mmol stearic acid, 20 mL dodecane, 0.1 g catalyst, 4 MPa H_2, T = 320 °C, and t = 8 h.
[b] The values in parentheses refer to the ratio of C17/(C18 + C18−OH) yields.
[c] Using water as the solvent.

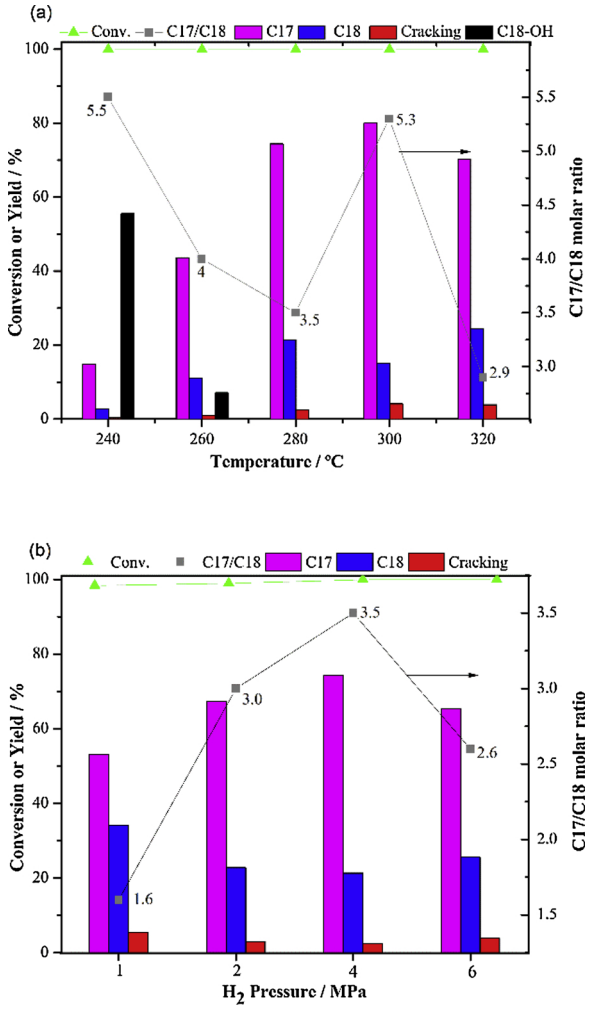

Fig. 5. Effect of reaction temperature (a) and H_2 pressure (b) on the conversion of stearic acid over (10 %)Co/N-C-550 catalyst. Reaction conditions: (a) 0.5 mmol stearic acid, 20 mL dodecane, 0.1 g (10 %)Co/N-C-550 catalyst, 4 Mpa H_2, t = 8 h. (b) 0.5 mmol stearic acid, 20 mL dodecane, 0.1 g (10 %)Co/N-C-550 catalyst, T = 280 °C.

decrease. Thus, a H_2 pressure of 4 MPa was used in subsequent experiments.

3.4. Effect of support

The effect of support has also been explored, as shown in Table 3. Al_2O_3 led to satisfactory yields of alkanes comparable to that of carbon-based catalyst but lower ratio of C17 to C18. Other metal oxide supports such as SiO_2, TiO_2, and ZrO_2 afforded much lower carbon balance. These metal-oxides-supported catalysts have much lower BET surface area and much larger average pore size than carbon-supported catalysts, so that the Co NPs are more likely to embed into the pore structure instead of on the surface like the Co-N-C catalyst, which are unfavorable for exposing of active centers towards HDO/DCOx reactions, leading to inferior catalytic performance.

The interaction between support and stearic acid to form carboxylate is often used to explain the good catalytic performance of metal oxide-supported metal catalysts for stearic acid conversion [11–13]. In this work, interaction between support and stearic acid is observed for Co/N-TiO_2 catalyst (Fig. S16), but not observed for Co/N-C catalyst. Meanwhile, the Co/N-C catalyst exhibited better catalytic performance than the Co/N-TiO_2 catalyst, suggesting that the typical interaction between the support and the stearic acid is not key for the catalytic performance of Co catalysts. This finding is consistent with our previous work about Ru-catalyzed conversion of fatty acids [13].

To further explore the reason for the good catalytic performance of Co/N-C catalyst, the Lewis acidity and basicity of some catalysts are examined (Fig. 6). It can be observed that only co-existence of Co and N-C leads to strong Lewis acidity and basicity, which is probably derived from Co NPs and nitrogen functionalities on the surface [13,53]. By comparison, the Co/N-TiO_2 catalyst only has Lewis basicity, which is important for the interaction between carboxylic acids substrate and catalyst as confirmed by FTIR. The additional Lewis acidity of Co/N-C catalyst promotes some important acid-catalyzed step-reactions such as oxygen removal during hydrogenation of carboxylic acid to aldehyde or deoxygenation of alcohol to alkane.

3.5. Reaction pathway

To explore the reaction pathways for Co-catalyzed conversion of stearic acid, the time course was recorded (Fig. 7a). It can be clearly seen that 1-octadecanol forms as the major intermediate reaching a

Table 3
Effect of support on the conversion of stearic acid over Co catalysts.[a]

Entry	Catalysts	BET Surface Area (m^2/g)	Average Pore Width (nm)	Conv. [%]	Yield[%]				C17/C18	Carbon balance
					n-C17	n-C18	C18-OH	Cracking products		
1	(10 %)Co/N-C-550	1004	4.58	> 99.9	74.3	21.3	0	2.5	3.5	98.1
2	(10 %)Co/N-Al_2O_3-550	17	11.83	98.7	58.5	32.4	0.1	6.1	1.8	98.4
3	(10 %)Co/N-SiO_2-550	156	21.45	77.1	1.3	0.5	19.6	0.5	2.6	28.4
4	(10 %)Co/N-TiO_2-550	54	15.65	99.6	2.3	9.2	2.3	0.7	0.3	14.6
5	(10 %)Co/N-ZrO_2-550	9	13.28	78.8	1.6	1.3	17.6	0.5	1.2	26.6

[a] Reaction conditions: 0.5 mmol stearic acid, 20 mL dodecane, 0.1 g catalyst, 4 MPa H_2, T = 280 °C, and t = 8 h.

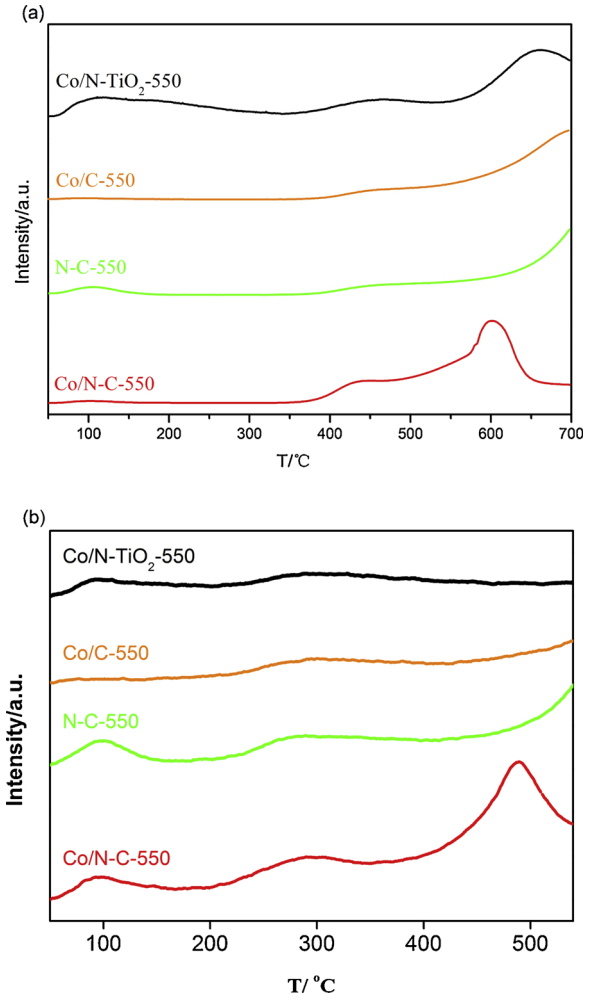

Fig. 6. (a) CO_2 and (b) NH_3-TPD of Co/N-TiO_2-550, Co/C-550, N-C-550, and Co/N-C-550 catalysts.

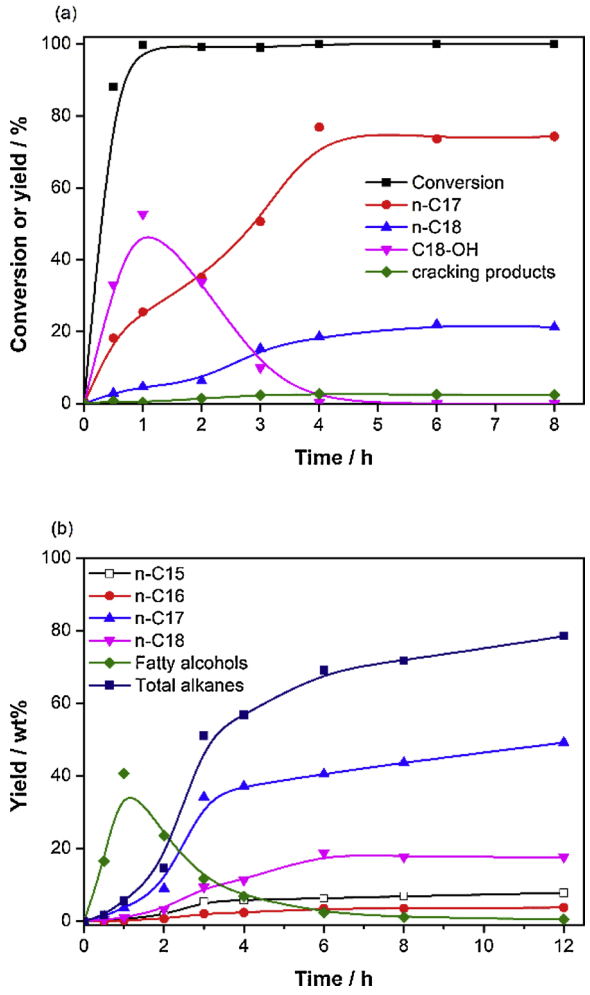

Fig. 7. Time course for the conversion of stearic acid (a) and cyperus esculentus oil (b) over (10 %)Co/N-C-550 catalyst. Reaction conditions: 0.5 mmol stearic acid or 200 mg cyperus esculentus oil, 20 mL dodecane, 0.1 g (10 %)Co/N-C-550 catalyst, T = 280 °C, 4 MPa H_2.

yield of 52.7 % in 1 h and is then consumed after 6 h. The conversion of 1-octadecanol involves two main pathways: 1) dehydrogenation followed by decarbonylation to major product C17; 2) dehydration followed by hydrogenation to minor product C18. The latter pathway is consistent with the acidity of the catalyst (Fig. 6b). Combined, our data support a picture of a bifunctional catalyst that consists of metallic and acidic active centers.

We also explored the conversion of triglycerides such as cyperus esculentus oil over Co/N-C, which showed similar transformation trends as the conversion of the stearic acid (Fig. 7b). Fatty alcohols are observed as major intermediates during the reaction, reaching a maximum yield of 40.7 wt% at 1 h, before they are completely consumed. After 12 h, the yield of liquid alkane reached 78.5 wt%, accounting for 95.5 % carbon in fatty acid groups of triglycerides. These results also demonstrate that the Co/N-C catalysts are very promising to catalyze the conversion of plant oils to liquid alkanes. Analysis of gaseous products showed that methane and ethane were generated with yields of 2.65 wt% and 0.45 wt%, respectively.

Besides the time course experiments, several model reactions were further explored to confirm the reaction pathway (left in Scheme 2). The alkane products are stable during reaction, i.e., C17 cannot be produced from cracking of C18. Reaction of stearic acid under N_2 still gave 13.5 % yield of C17, suggesting that decarboxylation probably occurs directly from the acid. No C18 is generated, demonstrating that H_2 is essential for the HDO reaction. Under H_2, 1-octadecanol gave 43.1 % yield of C17 and 4.3 % yield of C18 at complete conversion. The

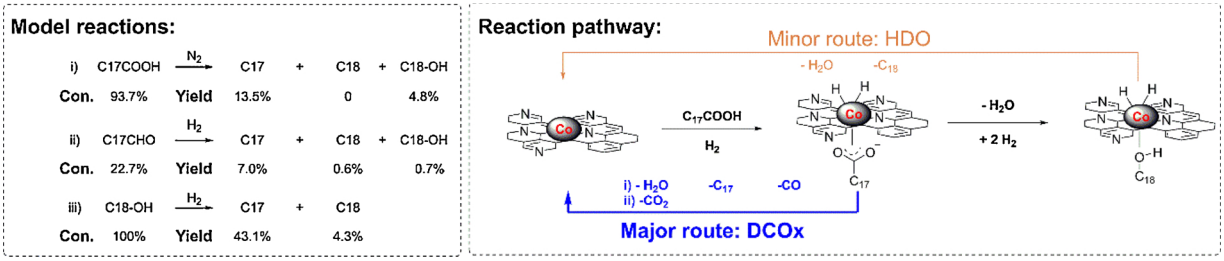

Scheme 2. Model reactions and proposed reaction pathways for the converstion of stearic acid over (10 %)Co/N-C-550 catalyst. Only when exposing the (111) facet of α-Co^0 is the DCOx route a major reaction route. The Co NPs act as Lewis base sites for the adsorption of stearic acid to form carboxylates, and act as Lewis acid sites for the adsorption of stearyl alcohol. Reaction conditions: i) 0.5 mmol stearic acid, 20 mL dodecane, 0.1 g (10 %)Co/N-C-550 catalyst, T = 280 °C, 4 MPa N_2, t = 8 h; ii) 0.25 mmol 1-octadecanal, 20 mL dodecane, 0.05 g (10 %)Co/N-C-550 catalyst, T = 280 °C, 4 MPa H_2, t = 0.5 h; iii) 0.5 mmol 1-octadecanol, 20 mL dodecane, 0.1 g (10 %)Co/N-C-550 catalyst, T = 280 °C, 4 MPa H_2, t = 8 h.

unsatisfactory carbon balance is probably due to the oligomerization of alkene intermediates to coke. 1-Octadecanal affords 7.0 % yield of C17, 0.6 % yield of C18, and 0.7 % yield of C18-OH at 22.7 % conversion. The DCOx dominant product distribution further confirmed that 1-octadecanal is the major intermediate during the conversion of stearic acid over Co-N-C catalysts.

By combining all of the above information, the proposed reaction pathway for Co/N-C-catalyzed conversion of fatty acids is shown in Scheme 2.

3.6. Recyclability

Stability is always an important factor of heterogeneous catalysts. For the conversion of carboxylic acids, slight loss of activity is observed in many metal catalysts such as Ru-La(OH)$_3$ [11], Ir-ReOx [14], Ni/B-MS catalysts [17], while significant loss of activity is observed for W_2C, Mo_2C [25], and Fe_3C catalysts [29]. For Co catalysis, only three work have reported the stability test results. The deactivation of Co/Al_2O_3 catalyst was observed after 100 h on-stream [20]. The deoxygenation activity of mesoporous zeolite(HZP-5 and -22)-supported Co catalyst is nearly unchanged during recycling tests, but the product distribution is changed [21,24].

In this work, the recyclability of Co/N-C catalyst was examined in five consecutive runs (Fig. 8). After each run, the used catalyst was separated by centrifugation followed by washing with dodecane, and then used directly in the next run. The catalytic activity of Co/N-C catalyst was maintained after the third cycle. Only ca. 1 % yield of 1-octadecanol is generated. The yield of 1-octadecanol slightly increased to 3.5 % in the fourth cycle, and then significantly increased to 20.3 % in the fifth cycle. The ICP-AES analysis showed that less than 0.005 % of initial Co is detected in the product solution, confirming no leaching of Co during recycle tests. Characterization of the reused catalyst by XPS indicated that the percent of Co^0 species dramatically decreased. The partial oxidation of metallic Co to Co oxides will weaken the oxophilic ability of Co NPs, thus resulting in inferior catalytic activity towards the conversion of carboxylic acids. XRD showed that the weak peak of the (111) facet of α-Co^0 species became broader and weaker after recycle tests (Fig. S17). In addition, the BET surface area, pore volume, and average pore width of the Co/N-C catalyst decreased after reusing (Table S6). Combined together, the inferior catalyst performance of Co-*N*-C catalyst after the fifth cycle is attributed to those structural changes.

3.7. Substrate scope

The substrate scope is examined through conversions of various long-chain fatty acids and methyl esters (Table 4). All the substrates gave excellent alkane yields, confirming the versatility of our Co/N-C catalyst. The results for oleic acid demonstrated that the DCOx/HDO of carboxyl group over Co/N-C catalyst proceeds well even in the presence

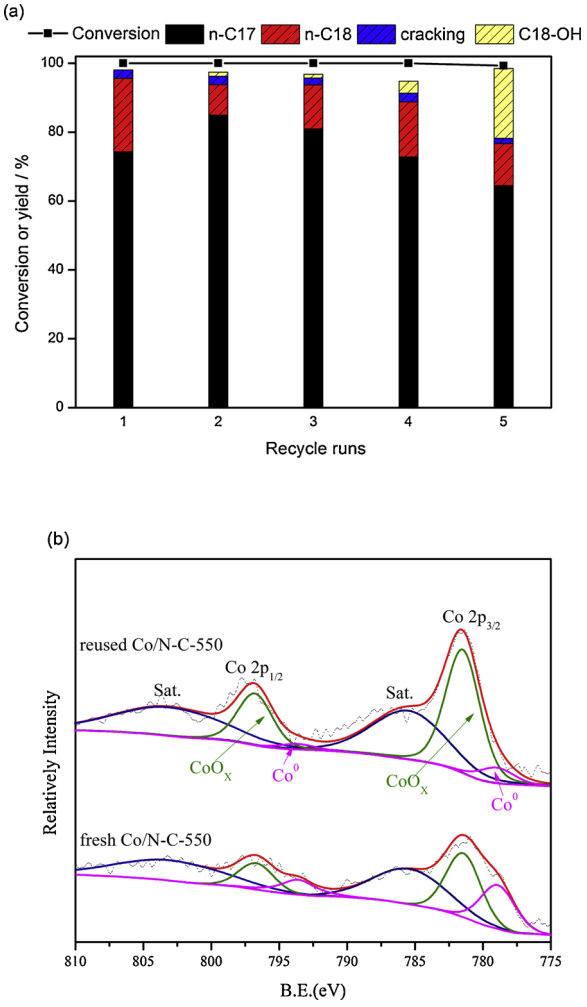

Fig. 8. (a) Recycling tests for the conversion of stearic acid over (10 %)Co/N-C-550 catalyst. Reaction conditions: 0.5 mmol stearic acid, 20 mL dodecane, 0.1 g Co/N-C-550 catalyst, T = 280 °C, 4 MPa H_2 and t = 8 h. (b) Co 2p XPS of fresh and reused Co/N-C-550 catalysts.

of C=C bond. The carbon chain length affects the DCOx/HDO selectivity when the carbon chain length decreased from 18 to 14, dropping from 2.9 to 1.9.

4. Conclusions

In this work, nitrogen-doped carbon supported Co^0 catalyst with an average particle size of 7.0 nm was synthesized via pyrolysis and found to be active towards the conversion of fatty acids and esters to liquid

Table 4
Conversion of various fatty acids/esters over (10 %)Co/N-C-550 catalyst.[a]

Entry	Substrate (X:Y)[b]	T [°C]	T [h]	Conversion [%]	Yield[%]		C_{n-1}/C_n
					C_{n-1}	C_n	
1	Stearic acid (18:0)	280	8	> 99.9	70.2	24.4	2.9
2	Methyl stearate (18:0)	280	8	> 99.9	70.1	22.3	3.1
3	Oleic acid (18:1)	280	8	> 99.9	71.8	21.9	3.3
4	Palmitic acid (16:0)	280	8	> 99.9	72	22.3	3.2
5	Methyl palmitate (16:0)	280	8	> 99.9	72.3	22.8	3.2
6[c]	Myristic acid (14:0)	280	8	> 99.9	62.8	32.3	1.9
7[c]	Methyl myristate (14:0)	280	8	> 99.9	67.3	28.2	2.4

[a] Reaction conditions: 0.5 mmol fatty acids/esters, 20 mL dodecane, 0.1 g (10 %)Co/N-C-550 catalyst.
[b] X represents the numbers of carbon, while Y represents the numbers of C=C bond.
[c] Decane is used as solvent to exclude interference from solvent during the determination of product yields.

alkanes. Nitrogen-doping facilitates a highly uniform dispersion of smaller Co NPs even at high metal loading of 10 wt% and stabilizes the catalyst against oxidation. It was shown that the pyrolysis temperature tunes the exposed facets which in turn control selectivity toward DCOx vs. HDO. Due to the partial reduction of Co oxides to α-Co^0 with only exposure of the (111) facet at a pyrolysis temperature of 550 °C, the Co/N-C catalyst promotes DCOx compared to previously reported Co catalysts. The NH_3- and CO_2-TPD profiles of Co/N-C-550 catalyst clearly showed that the co-existence of Co and N-C lead to significant Lewis acidity and basicity, facilitating the interaction between the carboxylic acids and some important acid-catalyzed reactions such as oxygen removal during hydrogenation of the carboxylic acid to an aldehyde or deoxygenation of the alcohol to an alkane. The versatility of Co/N-C catalyst was demonstrated through the effective conversion of various fatty acids and esters and plant oil. In order to better understand the relationship between the exposed facet and the selectivity, probe molecule chemistry and extensive DFT calculations will be needed as part of future work.

CRediT authorship contribution statement

Jiang Li: Conceptualization, Writing - original draft, Supervision, Funding acquisition. **Jiaxing Liu:** Methodology, Validation, Formal analysis, Investigation. **Junjie Zhang:** Formal analysis, Investigation. **Tong Wan:** Formal analysis, Investigation. **Lei Huang:** Investigation. **Xintian Wang:** Investigation. **Runze Pan:** Investigation. **Zhidong An:** Investigation. **Dionisios G. Vlachos:** Funding acquisition, Project administration, Writing - review & editing.

Acknowledgements

This work was supported by National Natural Science Foundation of China (21702227), Science Foundation of China University of Petroleum, Beijing (No.2462014YJRC037). DGV acknowledges support from the Catalysis Center for Energy Innovation, an Energy Frontier Research Center funded by the U.S. Department of Energy, Office of Science, Office of Basic Energy Sciences under Award number DE-SC0001004. Dr. Jiang Li also thanks the support of the China Scholarship Council (CSC).

Appendix A. Supplementary data

Supplementary material related to this article can be found, in the online version, at doi:https://doi.org/10.1016/j.apcata.2019.117385.

References

[1] G.W. Huber, S. Iborra, A. Corma, Chem. Rev. 106 (2006) 4044–4098.
[2] F. Jamil, L. Al-Haj, A.H. Al-Muhtaseb, M.A. Al-Hinai, M. Baawain, U. Rashid, M.N.M. Ahmad, Rev. Chem. Eng. 34 (2018) 267–297.
[3] C. Zhao, T. Bruck, J.A. Lercher, Green Chem. 15 (2013) 1720–1739.
[4] G.W. Huber, P. O'Connor, A. Corma, Appl. Catal. A Gen. 329 (2007) 120–129.
[5] D. Kubicka, L. Kaluza, Appl. Catal. A Gen. 372 (2010) 199–208.
[6] M. Anand, A.K. Sinha, Bioresour. Technol. 126 (2012) 148–155.
[7] B. Peng, Y. Yao, C. Zhao, J.A. Lercher, Angew. Chem. Int. Ed. 51 (2012) 2072–2075.
[8] B. Peng, X. Yuan, C. Zhao, J.A. Lercher, J. Am. Chem. Soc. 134 (2012) 9400–9405.
[9] Y. Shao, Q. Xia, X. Liu, G. Lu, Y. Wang, ChemSusChem 8 (2015) 1761–1767.
[10] K. Kon, W. Onodera, S. Takakusagi, K. Shimizu, Catal. Sci. Technol. 4 (2014) 3705–3712.
[11] J. Guo, G. Xu, F. Shen, Y. Fu, Y. Zhang, Q. Guo, Green Chem. 17 (2015) 2888–2895.
[12] G. Xu, Y. Zhang, Y. Fu, Q. Guo, ACS Catal. 7 (2017) 1158–1169.
[13] J. Li, S. Wang, H.Y. Liu, H.J. Zhou, Y. Fu, Chemistryselect 2 (2017) 33–41.
[14] S. Liu, T. Simonetti, W. Zheng, B. Saha, ChemSusChem 11 (2018) 1446–1454.
[15] K. Kandel, C. Frederickson, E.A. Smith, Y.J. Lee, I.I. Slowing, ACS Catal. 3 (2013) 2750–2758.
[16] W. Song, C. Zhao, J.A. Lercher, Chem. Eur. J. 19 (2013) 9833–9842.
[17] B. Ma, J. Hu, Y. Wang, C. Zhao, Green Chem. 17 (2015) 4610–4617.
[18] B. Ma, C. Zhao, Green Chem. 17 (2015) 1692–1701.
[19] E. Santillan-Jimenez, T. Morgan, J. Shoup, A.E. Harman-Ware, M. Crocker, Catal. Today 237 (2014) 136–144.
[20] A. Srifa, N. Viriya-empikul, S. Assabumrungrat, K. Faungnawakij, Catal. Sci. Technol. 5 (2015) 3693–3705.
[21] Y. Shi, E. Xing, Y. Cao, M. Liu, K. Wu, M. Yang, Y. Wu, Chem. Eng. Sci. 166 (2017) 262–273.
[22] V.K. Soni, P.R. Sharma, G. Choudhary, S. Pandey, R.K. Sharma, ACS Sustain. Chem. Eng. 5 (2017) 5351–5359.
[23] G. Wu, N. Zhang, W. Dai, N. Guan, L. Li, ChemSusChem 11 (2018) 2179–2188.
[24] M. Liu, Y. Shi, Y. Bi, E. Xing, Y. Wu, S. Huang, M. Yang, Energy Technol. 6 (2018) 406–415.
[25] R.W. Gosselink, D.R. Stellwagen, J.H. Bitter, Angew. Chem. Int. Ed. 52 (2013) 5089–5092.
[26] S.A.W. Hollak, R.W. Gosselink, D.S. Van Es, J.H. Bitter, ACS Catal. 3 (2013) 2837–2844.
[27] S.K. Kim, D. Yoon, S. Lee, J. Kim, ACS Catal. 5 (2015) 3292–3303.
[28] K. kandel, J.W. Anderegg, N.C. Nelson, U. Chaudhary, I.I. Slowing, J. Catal. 314 (2014) 142–148.
[29] J. Li, J. Zhang, S. Wang, G. Xu, H. Wang, D.G. Vlachos, ACS Catal. 9 (2019) 1564–1577.
[30] J. Deng, H. Song, M. Cui, Y. Du, Y. Fu, ChemSusChem 7 (2014) 3334–3340.
[31] X. Li, K. Zhang, S. Chen, C. Li, F. Li, H. Xu, Y. Fu, Green Chem. 20 (2018) 1095–1105.
[32] H. Zhou, J. Song, H. Fan, B. Zhang, Y. Yang, J. Hu, Q. Zhu, B. Han, Green Chem. 16 (2014) 3870–3875.
[33] P. Sun, G. Gao, Z. Zhao, C. Xia, F. Li, ACS Catal. 4 (2014) 4136–4142.
[34] L. Jiang, P. Zhou, C. Liao, Z. Zhang, S. Jin, ChemSusChem 11 (2018) 959–964.
[35] H. Yang, R. Nie, W. Xia, X. Yu, D. Jin, X. Lu, D. Zhou, Q. Xia, Green Chem. 19 (2017) 5714–5722.
[36] Y. Ma, G. Xu, H. Wang, Y. Wang, Y. Zhang, Y. Fu, ACS Catal. 8 (2018) 1268–1277.
[37] H. Luo, L. Wang, G. Li, S. Shang, Y. Lv, J. Niu, S. Gao, ACS Sustain. Chem. Eng. 6 (2018) 14188–14196.
[38] F.A. Westerhaus, R.V. Jagadeesh, G. Wienhofer, M. Pohl, J. Radnik, A. Surkus, J. Rabeah, K. Junge, H. Junge, M. Nielsen, A. Bruckner, M. Beller, Nat. Chem. 5 (2013) 537–543.
[39] D. Banerjee, R.V. Jagadeesh, K. Junge, M. Pohl, J. Radnik, A. Bruckner, M. Beller, Angew. Chem. Int. Ed. 53 (2014) 4359–4363.
[40] R.V. Jagadeesh, H. Junge, M. Pohl, J. Radnik, A. Bruckner, M. Beller, J. Am. Chem. Soc. 135 (2013) 10776–10782.
[41] F.K. Scharnagl, M.F. Hertrich, F. Ferretti, C. Kreyenschulte, H. Lund, R. Jackstell, M. Beller, Sci. Adv. 4 (2018) eaau1248.
[42] J. Masa, W. Xia, M. Muhler, W. Schuhmann, Angew. Chem. Int. Ed. 54 (2015) 10102–10120.
[43] Y. Cao, S. Mao, M. Li, Y. Chen, Y. Wang, ACS Catal. 7 (2017) 8090–8112.
[44] Z. Wei, J. Wang, S. Mao, D. Su, H. Jin, Y. Wang, F. Xu, H. Li, Y. Wang, ACS Catal. 5 (2015) 4783–4789.
[45] J.R. Pels, F. Kapteijn, J.A. Moulijn, Q. Zhu, K.M. Thomas, Carbon 33 (1995) 1641–1653.
[46] D. Guo, R. Shibuya, C. Akida, S. Saji, T. Kondo, J. Nakamura, Science 351 (2016) 361–365.
[47] J.H. Liu, T.K. Zhang, Z.C. Wang, G. Dawson, W. Chen, J. Mater. Chem. 21 (2011) 14398–14401.
[48] W. Ong, L. Tan, Y.H. Ng, S. Yong, S. Chai, Chem. Rev. 116 (2016) 7159–7329.
[49] X. Zhao, Q. An, Z. Xiao, S. Zhai, Z. Shi, Chem. Eng. J. 353 (2018) 746–759.
[50] M.C. Biesinger, B.P. Payne, A.P. Grosvenor, L.W.M. Lau, A.R. Gerson, R.S.C. Smart, Appl. Surf. Sci. 257 (2011) 2717–2730.
[51] S.A. Giles, Y. Yan, D.G. Vlachos, ACS Catal. 9 (2019) 1129–1139.
[52] X. Meng, Y. Yang, L. Chen, M. Xu, X. Zhang, M. Wei, ACS Catal. 9 (2019) 4226–4235.
[53] Y. Wang, J. Yao, H. Li, D. Su, M. Antonietti, J. Am. Chem. Soc. 133 (2011) 2362–2365.